A 2-D NAVIER-STOKES SOLUTION METHOD WITH OVERSET MOVING GRIDS

Ismail H. Tuncer*
Department of Aeronautics and Astronautics
Naval Postgraduate School, Monterey, California
Phone: 408/656-2854, Fax: 408/656-2313
tuncer@aa.nps.navy.mil, http://www.aa.nps.navy.mil/~tuncer

ABSTRACT

A simple, robust numerical algorithm to localize moving boundary points and to interpolate unsteady solution variables across 2-D, arbitrarily overset computational grids is presented. Overset grids are allowed to move in time relative to each other. The intergrid boundary points are localized in terms of three grid points on the donor grid by a directional search algorithm. The parameters of the search algorithm give the interpolation weights at the localized boundary point. The method is independent of numerical solution algorithms and may easily be implemented on any 2-D, single block flow solver to make it a multi-block, zonal solver with arbitrarily overset computational grids. Computational results and comparisons with single grid solutions are presented for flows through a compressor cascade and over an airfoil undergoing a flapping motion. Excellent agreement is obtained against the single grid solutions.

NOMENCLATURE

a	Speed of sound
c	Chord length
C_p	Pressure coefficient,$(p - p_{in})/\frac{1}{2}\rho_{in}V_{in}^2$
h	Flapping amplitude
k	Reduced frequency, $\omega c/2U_\infty$
M_∞	Free stream Mach number
P_0	Total pressure, Pascal
P_{in}	Inlet pressure, Pascal
Re	Reynolds number based on U_∞
t	Time
T_0	Total temperature, Kelvin
U_∞	Free stream velocity
V_{in}	Inlet velocity
α	Incidence angle, degrees
α_{in}	Inlet flow angle, degrees
ρ	Density
ρ_{in}	Density at the inlet
ω	Frequency
$+$	Intergrid boundary point to be localized
$\circ$	Donor grid points localizing the point $+$

INTRODUCTION

Among structured, block-structured and unstructured computational grids, structured grids still remain the most common in the CFD community (Thompson and Weatherhill, 1993). The basic advantage of the structured grids is that they are still the most suitable for the highly efficient solution algorithms developed and refined since the early establishment of the science of CFD. Due to the inherent connectivity information, numerical solution algorithms with structured grids are easy to implement on conventional, shared memory/multi–processor computers.

In discretizing complex geometries and irregular boundaries, the block–structured grid techniques (Steinbrenner et al., 1990; Thompson 1988), where a group of structured grid blocks are patched together with enforced continuity across the interfaces, are currently being utilized. Although the block-structured grids have all the inherent advantages of structured grids, they are not well suited for unsteady flow problems with moving boundaries, in which all the grid blocks need to be regenerated at every time step in order to satisfy the continuity across interfaces.

The recent applications of unstructured grids (Thomson and Weatherill, 1993; Steinbrenner et al., 1990; Thompson 1988; Barth and May, 1992) offer a promising alternative for treating irregular boundaries. However, for computation of unsteady flows with moving boundaries, the whole computational grid has to

*Research Assistant Professor

[0]This paper is declared a work of the U.S. Government and is not subject to copyright protection in the United States.

be regenerated at every time step similar to the block–structured grids. This process may become quite complex and costly (Morgan et al., 1992). Furthermore, the application of algebraic turbulence models in viscous flow problems, which utilizes the direction normal to solid surfaces, causes additional difficulties in unstructured grid topologies (Barth and May, 1992, Mavripilis, 1988).

The next alternative for treating complex geometries with moving boundaries is the use of overset grids, in which individual structured grids are overlaid on each other and free to move with respect to each other. In the present work, a new method is presented for the solution of the unsteady Navier-Stokes equations on overset structured grids, which are allowed to move relative to each other. The present method is similar to the Chimera/Pegsus (Benek, Buning and Steger, 1985) approach in essence. However, the two approaches differ in the way the overset boundaries are localized and the flow variables are interpolated.

In Pegsus, the localization of boundary points and the interpolation of flow variables across grid boundaries are done in several stages. First, all the grid points on the base grid are tested to determine if they lie within a certain distance from a temporary origin placed in the overset grid. All the grid points within the specified distance are next tested once more to see if they lie inside or outside of the overlapping grid boundary. The sign of the vector $\vec{N} \cdot \vec{R}$, where $\vec{R}$ is the relative position vector of the grid points and $\vec{N}$ is the unit outward normal at the cross-section of $\vec{R}$ and the intergrid boundary, determines the right direction. The closest points outside of the overlapping boundary are then assigned as the boundary points on the base grid. Finally, interpolation cells on the base grid, into which a boundary point of the overlapping grid falls, are localized, and the corresponding bilinear interpolation data are stored in an external file to be utilized by the flow solver. For unsteady flows, the Pegsus code has to be integrated into the flow solver and to be executed at every time step.

In the present method, the boundary point localization and interpolation of flow variables are integrated into a directional search algorithm in the main flow solver. The directional search algorithm localizes the boundary points on the donor grid and provides the interpolation weights. No external data is stored. In an earlier work (Tuncer, 1996) the method has been applied to airfoil flows with overlapping and overset grids. In this work, it is extended to cascade flows and to a high frequency flapping motion of an airfoil.

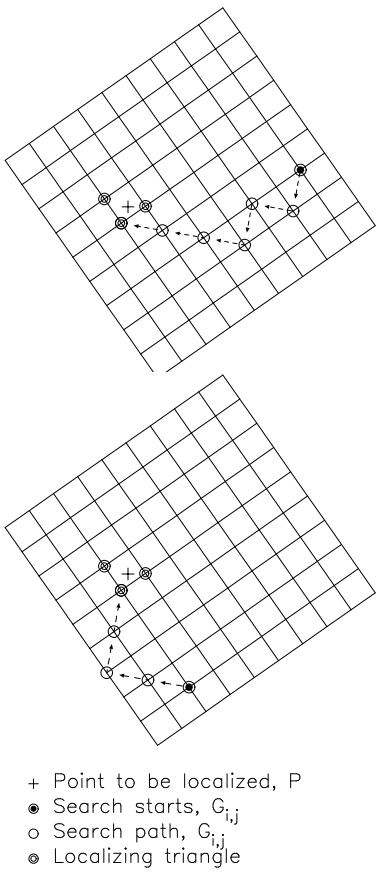

Fig. 1a Localization of a point

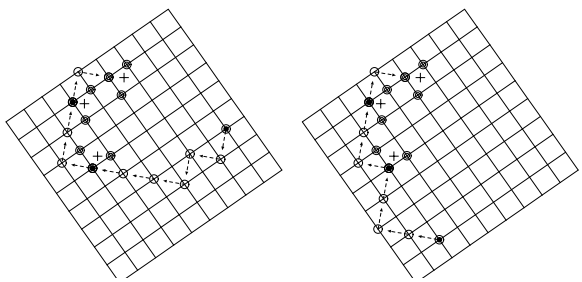

Fig. 1b Sequential localization of points

BOUNDARY POINT LOCALIZATION

In the present approach, the intergrid boundary points are localized on the adjacent/donor grids with a directional search algorithm. The directional search process is depicted in Figure 1. Here, a single point, P, denoted by the + sign, is localized on a Cartesian grid in terms of the three closest grid points, which constitute a triangle. The search process starts from an arbitrary grid point $G_{i,j}$ as denoted by a double solid circle in the figure. It is then tested to see if the point P falls into the triangle defined by grid points at $G_{i,j}, G_{i\pm1,j}$ and $G_{i,j\pm1}$, where the correct sign $\pm$ is determined by the

search direction. The search direction is based on the geometry gradients on the grid. The test whether the point P falls into the triangle is based on the representation of a convex surface defined by the three points and determined by the solution of the following three linear equations in terms of α, β and γ. Since any point in a convex triangular surface may uniquely be represented by three real numbers provided that they are all positive.

$$\begin{aligned} P(x,y) &= \alpha G_{i,j} + \beta G_{i\pm1,j} + \gamma G_{i,j\pm1} \\ 1 &= \alpha + \beta + \gamma \end{aligned}$$

Note that the first vector equation has two components for x and y. If the coefficients α, β and γ are all positive, then the point P lies inside the triangle. If not, the search location $G_{i,j}$ is advanced along the grid lines as shown by arrows and circles in Figure 1. Finally, the triangle into which the point P falls is localized as depicted by the circles at its vertices. Once the point is localized, the coefficients α, β and γ give the geometric interpolation weights at the point P in terms of the function values at the three interpolation points. Thus, interpolation weights are readily available to interpolate flow variables at the point P from the donor grid.

The directional search process with a different starting point is also depicted in Figure 1a. The sequential localization of several points is depicted in Figure 1b. As shown, the search process for localizing the next consecutive point starts from the $G_{i,j}$ grid point which localizes the previous point.

In this work, the localization process is applied to moving overset grids. The boundary point localization and the interpolation of flow variables are performed at every time step as the computational grids move relative to each other in an unsteady motion. The localization process gives the interpolation weights. Thus, the flow variables at the intergrid boundary points may be interpolated from the donor grid simultaneously. Since the intergrid boundary points are localized sequentially and the localization algorithm is unified with the interpolation scheme, the application of the intergrid boundary conditions becomes quite robust and efficient. It should also be noted that no interpolation data needs to be stored. Flow variables are interpolated across overset grids as an integral part of the localization of intergrid boundary points.

NAVIER–STOKES SOLVER

An implicit, thin–layer, Navier-Stokes solver (Tuncer et al., 1996, 1995, 1995) with the third order accurate Osher's upwind biased flux difference splitting scheme is employed to compute the flowfield in each computational grid. The strong conservation–law form of the 2–D, thin–layer Navier–Stokes equations in a curvilinear coordinate system, (ξ, ζ), along the axial and normal direction respectively, is given as follows

$$\partial_t \hat{\mathbf{Q}} + \partial_\xi \hat{\mathbf{F}} + \partial_\zeta \hat{\mathbf{G}} = Re^{-1} \partial_\zeta \hat{\mathbf{S}} \qquad (1)$$

where $\hat{\mathbf{Q}}$ is the vector of conservative variables, $1/J(\rho, \rho u, \rho w, e)$, $\hat{\mathbf{F}}$ and $\hat{\mathbf{G}}$ are the inviscid flux vectors, and $\mathbf{S}$ is the thin layer approximation of the viscous fluxes in the ζ direction normal to the airfoil surface. The pressure is related to density and total energy through the equation of state for an ideal gas, $p = (\gamma - 1)\left[e - \rho(u^2 + w^2)/2\right]$.

The flowfield is assumed to be fully turbulent and the Baldwin–Lomax turbulence model is implemented.

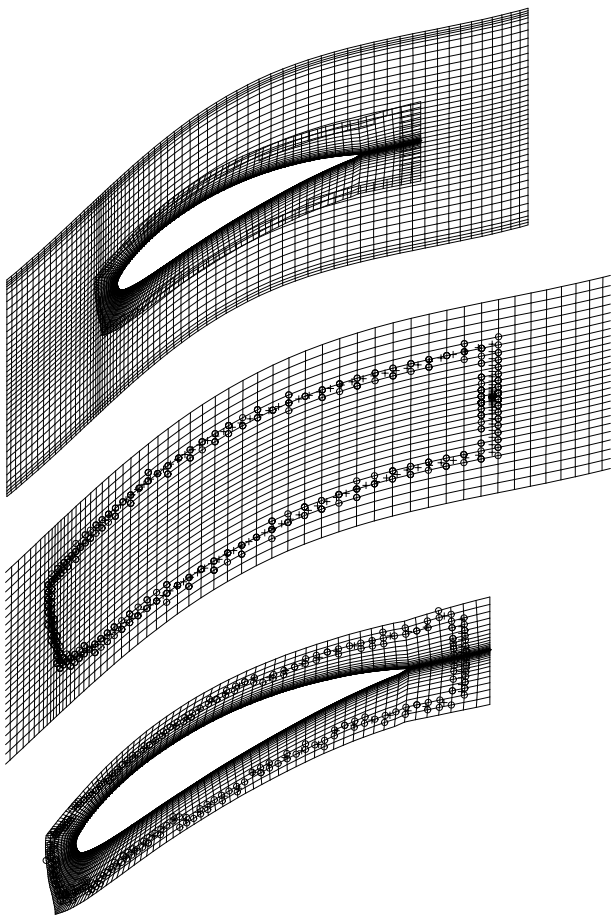

Fig. 2 Overset grids for the annular compressor cascade and localization of the intergrid boundary points.

Boundary Conditions

On the airfoil surfaces the no–slip boundary condition is applied. For the flapping airfoil, the surface fluid velocity is set equal to the prescribed airfoil flapping velocity. Since the formulation of the Navier-Stokes solver is based on an inertial frame of reference, the flapping motion of the airfoil is implemented by moving the airfoil and the computational grid around it in the cross-flow direction. The density and pressure values on the airfoil surface are extrapolated from the interior solution.

At the intergrid boundaries, the conservative flow variables are interpolated at every time step using the present boundary point localization and interpolation method.

At the farfield inflow and outflow boundaries the flow variables are evaluated using the zero–order Riemann invariant extrapolation.

In cascade flows, at the inlet, the density values are extrapolated from the interior solution. The rest of the flow variables are obtained through the application of the Riemann invariant extrapolation and the isentropic flow relations which relate the total temperature and pressure to velocity. Periodic boundary conditions are imposed by alternatingly extrapolating the flow variables from the interior solution at the lower and upper boundaries.

Numerical Implementation

The numerical integration in each computational grid is performed using an upwind biased, factorized, iterative, implicit, numerical scheme given by

$$
\begin{aligned}
&\left[I + h_\xi \left(\nabla_\xi^b \tilde{A}_{i,k}^+ + \Delta_\xi^f \tilde{A}_{i,k}^-\right)\right]^p \\
&\quad \times \left[I + h_\zeta \left(\nabla_\zeta^b \tilde{B}_{i,k}^+ + \Delta_\zeta^f \tilde{B}_{i,k}^- - Re^{-1}\delta_\zeta \tilde{M}_{i,k}\right)\right]^p \\
&\quad \times \left(\tilde{Q}_{i,k}^{p+1} - \tilde{Q}_{i,k}^p\right) \qquad (2) \\
= \; &-\left[\left(\tilde{Q}_{i,k}^p - Q_{i,k}^n\right)\right. \\
&\quad + h_\xi \left(\hat{F}_{i+1/2,k}^p - \hat{F}_{i-1/2,k}^p\right) \\
&\quad + h_\zeta \left(\hat{G}_{i,k+1/2}^p - \hat{G}_{i,k-1/2}^p\right) - \\
&\quad \left. - Re^{-1} h_\zeta \left(\hat{S}_{i,k+1/2}^p - \hat{S}_{i,k-1/2}^p\right)\right]
\end{aligned}
$$

In Eq. (2), $h_\xi = \Delta\tau/\Delta\xi$ etc. and $\tilde{A}^\pm = (\partial\tilde{F}/\partial\tilde{Q})$ etc. are the flux Jacobian matrices, and Δ, ∇, and δ are the forward, the backward and the central difference operators, respectively. The quantities $\tilde{F}_{i+1/2,k}$ and $\tilde{G}_{i,k+1/2}$ and $\tilde{S}_{i,k+1/2}$ are numerical fluxes. The superscript ^{n} denotes the time step and ^{p} refers to Newton subiterations within each time step.

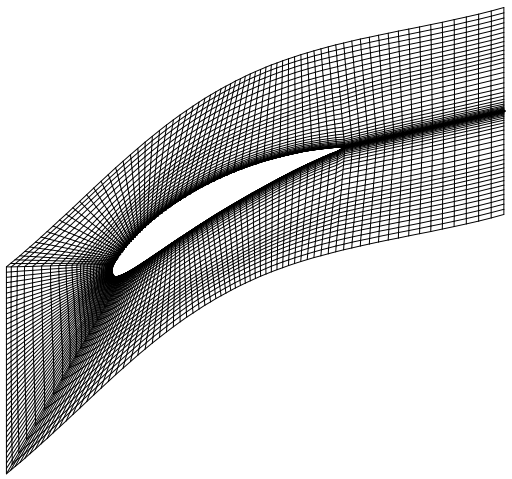

Fig. 3 A single C–grid for the annular compressor cascade.

The inviscid fluxes $\hat{F}$ and $\hat{G}$ are evaluated using Osher's third–order–accurate upwinding scheme. For the linearization of the left–hand side of Eq. (2) the flux Jacobian matrices A, B are evaluated by the Steger–Warming flux–vector splitting. The viscous fluxes $\hat{S}$ are computed with second–order–accurate central differences.

The numerical integration at the hole points is accommodated by replacing the corresponding coefficient matrices by an identity matrix and by setting the right hand side to zero. This process essentially imposes no change in the flow variables on the hole grid points.

RESULTS AND DISCUSSION

In this study, the present boundary point localization and interpolation method was applied to an annular compressor cascade (Schulz and Gallus, 1988) and to a single NACA0012 airfoil undergoing a sinusoidally flapping motion. The computational domains are discretized with two overset subgrids. A C–grid around the airfoil is overset onto a rectangular base grid. The solutions obtained with overset grids are compared against single grid solutions.

The overhead due to the application of the intergrid boundary conditions is about 0.2% of the total CPU per time step. It should be noted that since the

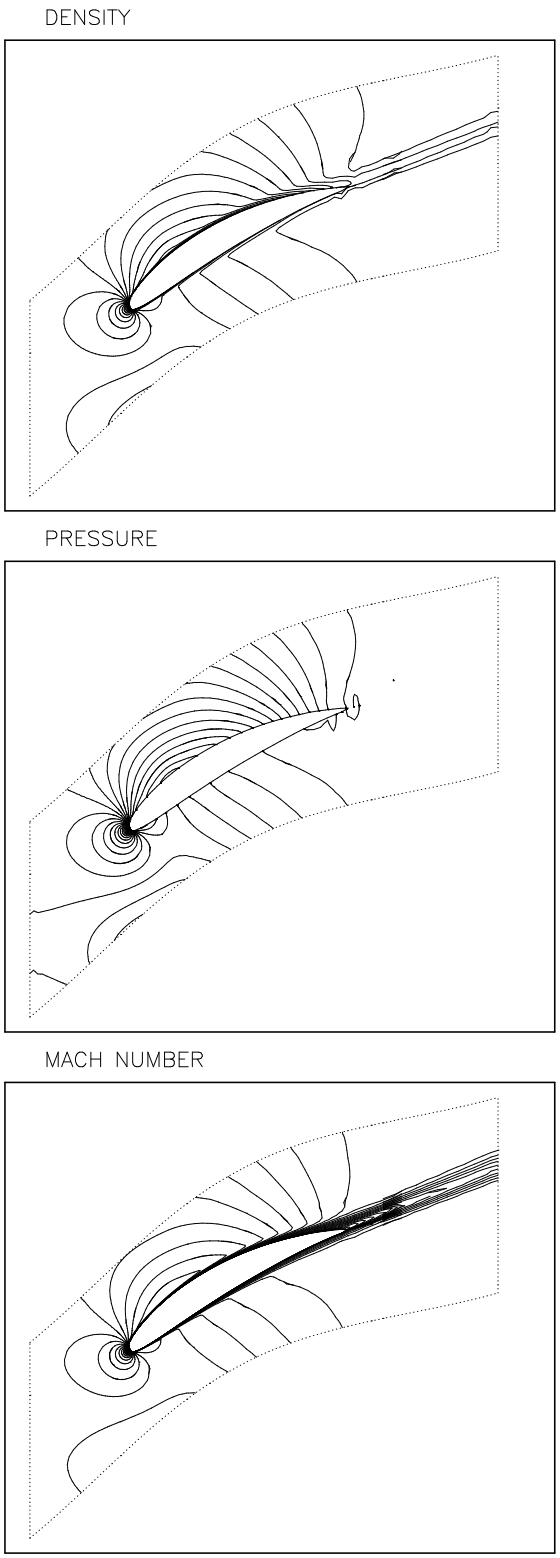

Fig. 4 Steady flowfield computed on the overset grid - Annular compressor cascade, $\alpha_{in} = 43.85°$, $P_0 = 106600\ Pa$, $T_0 = 303.7°K$, and $P_{exit} = 101900\ Pa$

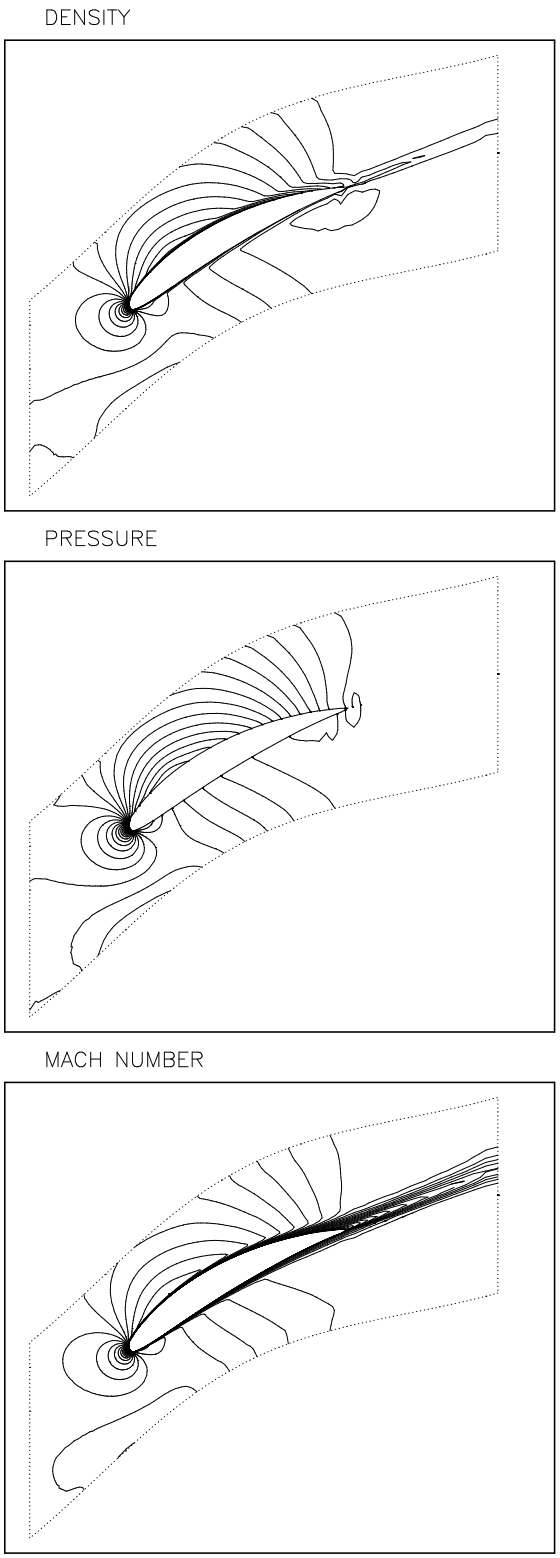

Fig. 5 Steady flowfield computed on the single C–grid - Annular compressor cascade, $\alpha_{in} = 43.85°$, $P_0 = 106600\ Pa$, $T_0 = 303.7°K$, and $P_{exit} = 101900\ Pa$

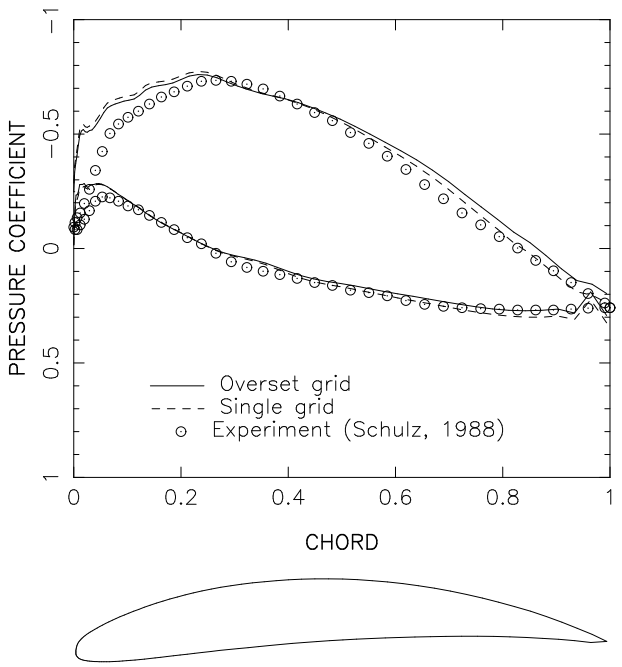

Fig. 6 Surface pressure distribution - Annular compressor cascade, $\alpha_{in} = 43.85°$, $P_0 = 106600\ Pa$, $T_0 = 303.7°K$, and $P_{exit} = 101900\ Pa$

equations are solved implicitly with a block-tridiagonal solver, single grid solutions are more CPU intensive per time step than overset grid solutions with the same total number of grid points.

Compressor Cascade

The flow conditions for the annular compressor cascade are specified as $\alpha_{in} = 43.85°$, $P_0 = 106600\ Pa$, $T_0 = 303.7°K$, and $P_{exit} = 101900\ Pa$.

In Figure 2, the overset grid system and the localization of the intergrid boundary points are shown. A 163×29 size viscous C–grid around the blade is overset onto a clustered 71×41 size rectangular base grid. There are 145 grid points around the blade and the grid spacing normal to the blade surface varies from $y^+ = 0.5$ at the trailing edge to $y^+ = 3.0$ at the leading edge. As shown in Figure 2b, the outer boundary points of the overset C–grid, which are denoted by the + sign, are first localized sequentially on the base grid. This process defines the initial boundary points of the hole cut in the base grid. In this study, the overlapping intergrid region was enlarged by extending the boundaries of the hole on the base grid by one grid point inward in both i and j directions. This process ensures that all the boundary points defining the hole fall into the C–grid. An indexing array is utilized to denote the hole points on the base grid. Next, as shown in Figure 2c, the boundary points of the extended hole on the base grid are localized on the C–grid.

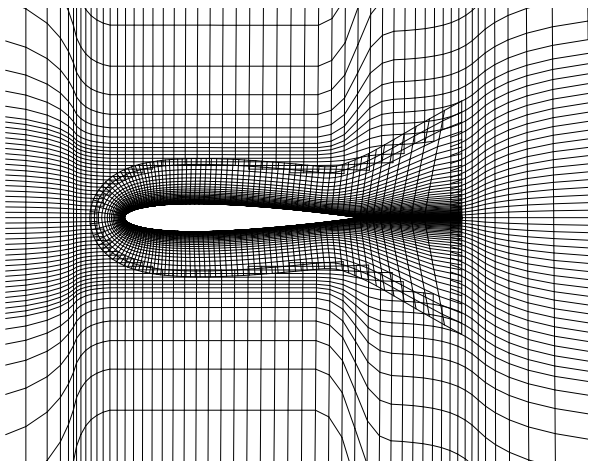

Fig. 7 Overset grids around a NACA0012 airfoil.

A single C–grid, shown in Figure 3, is employed for a single grid solution. It is of 181x41 size and is obtained by extending the C–grid used in the overset grid system to the periodic boundaries.

In Figures 4 and 5, the flowfields computed on the overset grid and on a single C–grid are given. The same contour levels are plotted in both cases. As seen in figure 4, the contour lines of the flow variables are continuous across the intergrid boundaries and are in good agreement with the single grid solution, which indicate that the flow variables are accurately interpolated across the intergrid boundaries. Figure 6 shows the comparison of surface pressures. The disagreement between computed and experimental data at the leading edge of the blade may be attributed to the transition and turbulence modeling (Sanz and Platzer, 1996). Although the overset grid and the single C–grid predictions agree in general, it should be noted that periodic boundaries are resolved better with the overset grid. Further grid studies are needed to identify the grid dependency of the solution on the application of periodic boundary conditions.

Flapping Airfoil

Next, a similar overset grid system (Fig. 7) is employed for an unsteady flow solution over an NACA0012 airfoil undergoing a periodic flapping motion. The flapping motion is defined by $h = -0.10c\cos(\omega t)$ at a reduced frequency of $k = \omega c/2U_\infty = 1.0$.

As the airfoil undergoes the prescribed flapping motion, the overset C–grid moves in time relative to the

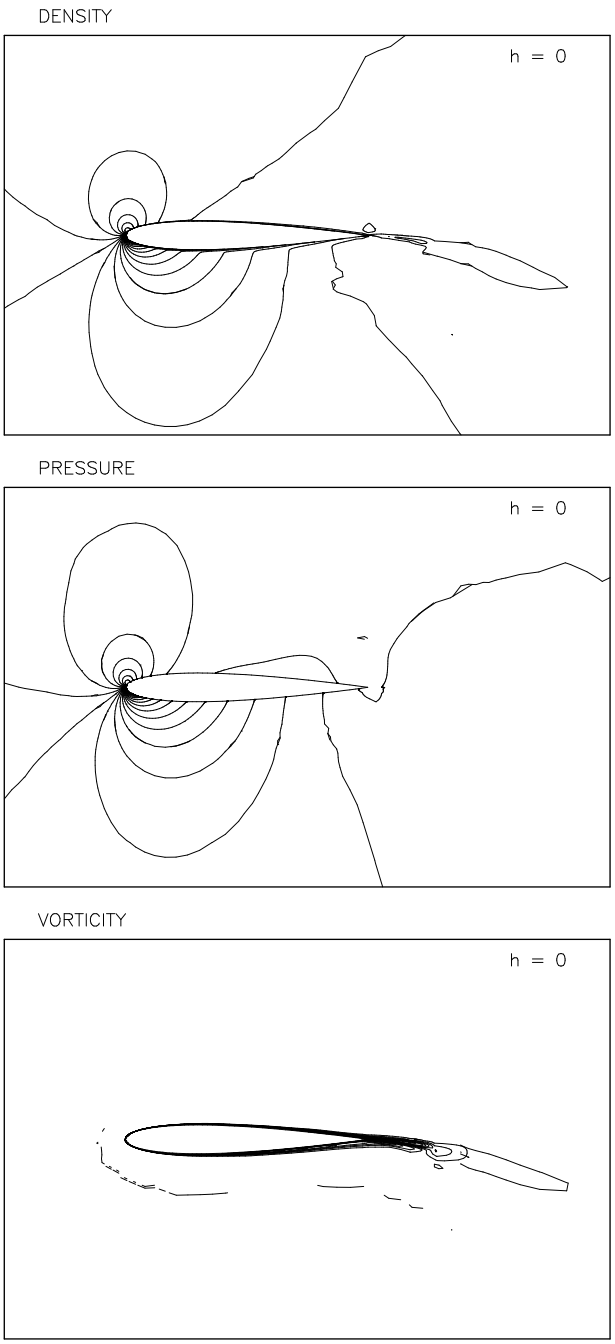

Fig. 8 Instantaneous flowfield computed on the overset C–H grid at $tU_\infty/c = 14.10, h = 0.0$ - Flapping NACA0012 airfoil with $h = -0.10c\cos(\omega t)$, $k = 1.0$, $M_\infty = 0.3$, $Re = 3 \cdot 10^6$.

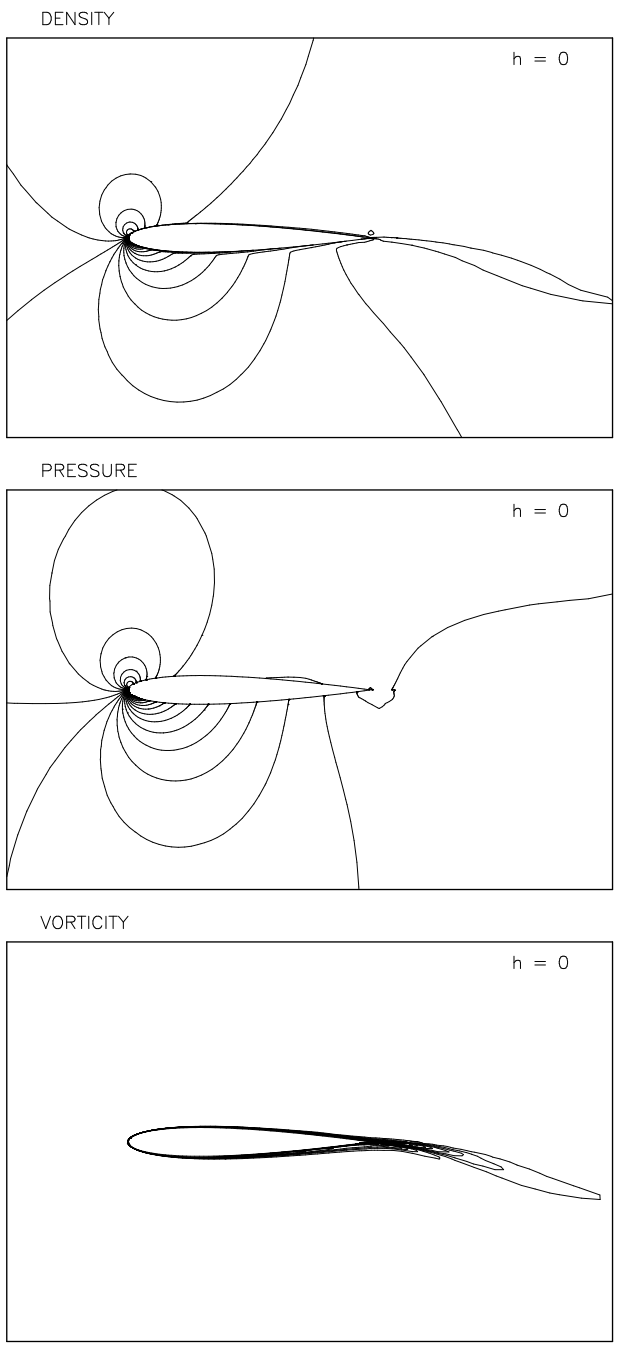

Fig. 9 Instantaneous flowfield computed on a single C grid at $tU_\infty/c = 14.10, h = 0.0$ - Flapping NACA0012 airfoil with $h = -0.10c\cos(\omega t)$, $k = 1.0$, $M_\infty = 0.3$, $Re = 3 \cdot 10^6$.

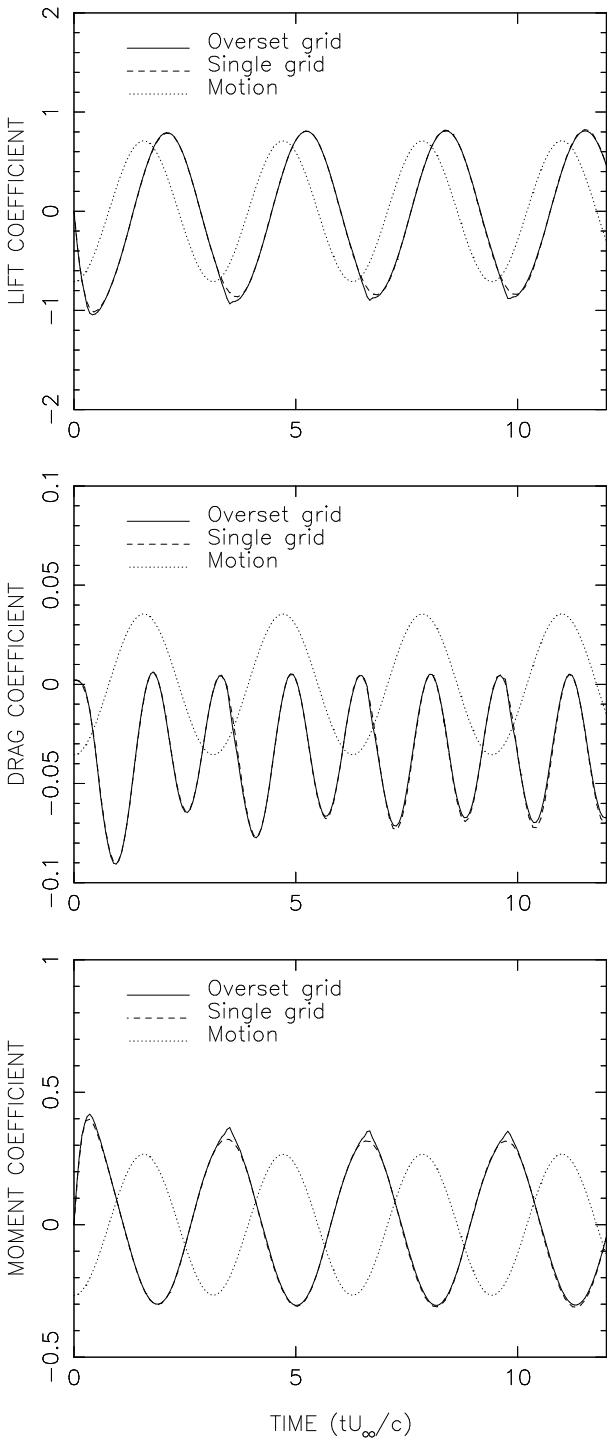

Fig. 10 Time history of the unsteady aerodynamic loads - Flapping NACA0012 airfoil with $h = -0.10c\cos(\omega t)$, $k = 1.0$, $M_\infty = 0.3$, $Re = 3 \cdot 10^6$.

base grid in the cross-flow direction. In Figures 8 and 9, the instantaneous flowfield as the airfoil passes the $h = 0$ position with the maximum velocity is similarly compared against the single grid solution. In vorticity contours, it is seen that the vorticity interpolated from the highly clustered C–grid at the downstream end of the wake onto the coarser base grid gets diffused on the base grid. The comparison of unsteady aerodynamic loads is given in Figure 10. It should be noted that the flapping motion produces thrust (Tuncer and Platzer, 1996). As seen, the overset grid solution agrees well with the single grid solution at the high frequency grid motions. However, in comparison to a low frequency flapping motion (Tuncer, 1996), the accuracy of the predictions deteriorates slightly.

CONCLUDING REMARKS

A new method for the solution of unsteady Navier-Stokes equations on overset grids is presented. In this method, intergrid boundary points are localized by a directional search algorithm and flow variables across the grids are interpolated as an integral part of the boundary point localization process in the main solver. No external interpolation data is stored. Computed flow variables are continuous across the overset grid boundaries and steady and unsteady flowfield solutions were found to be in excellent agreement with the single grid solutions. The CPU overhead due to the application of the overset grid boundaries is less than 0.2% per time step. Therefore, the application of the intergrid boundary conditions with the present boundary point localization and interpolation method is highly accurate and robust.

It should also be noted that the present boundary point localization and interpolation method is independent of the numerical solution algorithm employed. It may easily be implemented on any 2-D, single block flow solver to make it a multi-block, zonal solver regardless of the solution algorithm and the flow variables employed.

REFERENCES

Barth, J.T., May 1992, *Aspects of Unstructured Grids and Finite–Volume Solvers for Euler and Navier–Stokes Equations,* AGARD Report 787, Special course notes.

Benek, J.A., Buning P.G. and Steger J.L., 1985, *A 3-D Chimera Grid Embedding Technique*, AIAA paper 85–1523.

Mavripilis, D., 1988, *Adaptive Mesh Generation for Viscous Flows Using Delaunay Triangulation,*, ICASE Repost No. 88-47.

Morgan, K, Perarie, J. and Perio, J., May 1992, *Unstructured Grid Methods for Compressible Flows,* AGARD Report 787, Special course notes.

Sanz, W., and Platzer, M.F., 1996, *On the Navier-Stokes Calculation of Separation Bubbles with a new Transition Model*, ASME paper, to be presented at the Turbo Expo'96 meeting.

Schulz, H.G. and Gallus, H.E., 1988, *Experimental Investigation of the Three-Dimensional Flow in an Annular Compressor Cascade*, ASME Journal of Turbomachinery , Vol. 110.

Steinbrenner, J.P., Chawner, J.R. and Fouts, C.L., 1990, *Multiple Block Grid Generation in the Interactive Environment.*, AIAA Paper 90–1602.

Thompson, J.F. 1988, *Composite Grid Generation Code for General 3-D Regions – the EAGLE Code,*, AIAA Journal, 26.3: 271-272.

Thompson, J.F. and Weatherill, N.P, August, 1993, *Aspects of Numerical Grid Generation: Current Science and Art,* AIAA Paper 93-3539-CP, Applied Aerodynamics Conference.

Tuncer, I.H. and Platzer, M.F., February 1996, *Thrust Generation due to Airfoil Flapping,* AIAA Journal, Vol. 34, No. 2, pp. 324-331.

Tuncer, I.H and Platzer, M.F., 1995, *Analysis of Unsteady Airfoil Interference Effects Using a Zonal Navier-Stokes Solver*, AIAA paper 95–0307.

Tuncer, I.H, Ekaterinaris, J.A. and Platzer, M.F., January 1995, *A Viscous-Inviscid Interaction Method for Unsteady Low Speed Airfoil Flows,* AIAA Journal, Vol. 33, No. 1, pp. 151-154.

Tuncer, I.H, January 1996, *A 2–D Unsteady Navier–Stokes Solution Method with Overlapping, Overset Moving Grids*, AIAA paper 96–0822.